Acta Acustica 2022, **6**, 24

https://doi.org/10.1051/aacus/2022019

Available online at:
https://acta-acustica.edpsciences.org

SCIENTIFIC ARTICLE OPEN ACCESS

Acoustic scattering effect prediction of helicopter fuselage based on BEM and convective FW–H equation

Zeyang Wang, Jun Huang, and Mingxu Yi*

Beihang University, 100191 Beijing, China

Received 9 November 2021, Accepted 18 May 2022

Abstract – The main acoustic noise source of helicopters is supposed to be the rotor blades, but the scattering effect of the helicopter fuselage sometimes cannot be ignored. For the accuracy of acoustic noise prediction and the research on the scattering affections of the helicopter fuselage, an FWH–BEM Method (FBM) based on convective FW–H equation and boundary element method (BEM) is presented for the prediction of the noise scattering effects of helicopter fuselage and the approach to the calculation of a helicopter's acoustic noise field. In this paper, different fuselage models are adopted for the comparisons of the acoustic noise scattered by different types of fuselages. According to the discovery that helicopter fuselages with sharp edges can bring more significant acoustic scattering effects, a research on the influence of radius of curvature (RC), which reflects the sharpness of fuselage sharp edges, is also carried out. In addition, the acoustic scattering effects of the same type of fuselage but with different length, width and height ratios are also compared for discovering the influences of the fuselage size. The presented FBM is efficient to analyze the acoustic scattering effects of the helicopter fuselage and predict the acoustic noise field, taking both the rotor and the fuselage into account. Besides, the research in this paper leads to the discovery of the influence factors of the acoustic scattering effects and helps the proper selection of the fuselage in a helicopter stealth design.

Keywords: Convective FW–H equation, Boundary Element Method, Acoustic scattering effects, Fuselage, Sound pressure level

1 Introduction

The most important characteristic signal of helicopters is acknowledged to be acoustic noise, which can be a severe problem of the acoustic stealth of helicopters. Therefore it is essential that a proper stealth design is adopted for a new helicopter, aiming at suppressing its acoustic noise and strengthening its acoustic stealth ability [1–3].

Predicting the acoustic noise [4–6] is one of the important parts of aircraft acoustic stealth technology, helping to ascertain the sound pressure level of acoustic noise and find out the main affection factors. It is commonly acknowledged that the rotor blades are regarded as the main acoustic noise source of a helicopter, whose acoustic noise prediction problem can be regarded as the calculation of the sound field of rotating sound sources. The Ffowcs Williams and Hawkings (FW–H) equation [7] is a standard approach to the solutions of this sort of problems. Taking account of the influence of medium movement (inflow), Ghorbaniasl and Lacor [8] have developed a direct calculation method of the sound field of rotating sound sources with inflow, based on convective FW–H equation, and also developed several time domain formulations for the solution of the convective FW–H equation. Ghorbaniasl *et al.* [9] and Huang *et al.* [10] have deduced convective Kirchhoff equation for the calculation of sound field.

However, not all of the sound waves travel directly in straight lines to infinity, for the existence of helicopter fuselage that brings acoustic scattering effects for its reflection of sound waves. Therefore a method is required for the calculation of the acoustic scattering effects of the helicopter fuselage. Common methods include equivalent source method (ESM) and boundary element method (BEM) [11–13]. Compared with ESM that should disperse the whole domain, BEM just requires the dispersal of the boundary, transferring three dimensional problems into two-dimensional problems so that the complexity and workload can be reduced. The helicopter fuselage can be regarded as a solid boundary and thus BEM method can be a proper method adapted to the calculation of its acoustic scattering effects.

Some basic researches based on boundary element method (BEM) have been brought out for calculations of acoustic scattering effects. Roger Michel and Kucukcoskun Korcan [14] studied the scattering effects of the solid strut member of a rotor and put forward some relevant theories. Seongkyu Lee, Kenneth Brentner and Philip Morris [15, 16] studied the scattering effects in the time domain using an equivalent source method, with a sphere solid scattering

*Corresponding author: yimingxu@buaa.edu.cn

boundary and a point sound source. Curle [17] studied the influence of solid boundaries upon aerodynamic sound and the acoustic scattering effects of the solid boundaries.

Previous researches mainly focus on the theories of BEM method [18–20], and some basic verification cases of acoustic scattering effects with simple solid boundaries such as spheres and plains [21, 22]. The research presented in this paper aims at the acoustic scattering effects of the acoustic noise produced by the helicopter rotor blades with the solid boundary of helicopter fuselage, and tries to discover the influence of the variety of the fuselage types and sizes.

This research is presented in three sections. In the first section, a method based on BEM method and convective FW–H equation is presented. In the second section, helicopter models with different types of fuselages are established for the research on the influence on acoustic scattering effects of different fuselage types. In the third section, we make a research on the influence of the length, width and height of the fuselage and summarize the rules of the elements' influence.

2. Theoretical background

2.1 Convective FW–H equation

Fundamental equations of fluid flow in an unbounded region outside the control surface without external force can be described as [7]

$$\frac{\partial \rho}{\partial t}+\frac{\partial \rho u_i}{\partial x_i}=0, \tag{1}$$

$$\frac{\partial \rho u_i}{\partial t}+\frac{\partial \rho u_i u_j}{\partial x_j}-\frac{\partial P_{ij}}{\partial x_j}=0, \tag{2}$$

where ρ is the density of the fluid, u_i is the velocity of the fluid, and P_{ij} is the tensor of the force loading on the fluid. Equation (1) is known as the continuity equation and equation (2) is known as the momentum equation.

With the utilization of Heaviside Function, the continuity equation can be adapted as

$$\frac{\partial}{\partial t}[p'H(f)]+\frac{\partial}{\partial x_j}[\rho u_i H(f)]=\rho_0 u_i\frac{\partial H}{\partial x_i}=\rho_0 v_n|\nabla f|\delta(f), \tag{3}$$

where

$$H(f)=\begin{cases}1, & f(x,t)>0\\ 0, & f(x,t)<0\end{cases} \tag{4}$$

$H(f)$ is known as Heaviside Function.

Similarly, the momentum equation can be rewritten as

$$\frac{\partial}{\partial t}[\rho u_i H(f)]+\frac{\partial}{\partial x_i}\left[\left(-P_{ij}+\rho u_i u_j\right)H(f)\right] =-P_{ij}n_j|\nabla f|\delta(f)=-P_{ij}\frac{\partial f}{\partial x_j}\delta(f). \tag{5}$$

Let $T_{ij}=-P_{ij}+\rho u_i u_j-c_0^2\rho'\delta_{ij}$, we can obtain that

$$\left(\frac{1}{c_0^2}\frac{\partial^2}{\partial t^2}-\frac{\partial^2}{\partial x_i^2}\right)[p'H(f)]=\frac{\partial}{\partial t}\left[\rho_0 v_i\frac{\partial f}{\partial x_i}\delta(f)\right] -\frac{\partial}{\partial x_i}\left[-P_{ij}\frac{\partial f}{\partial x_i}\delta(f)\right]+\frac{\partial^2}{\partial x_i\partial x_j}\left[T_{ij}H(f)\right], \tag{6}$$

which is acknowledged as FW–H equation.

The acoustic solution of FW–H equation can be obtained as [11–13]

$$p'(x,t)=p'_T(x,t)+p'_L(x,t), \tag{7}$$

where $p'_T(x,t)$ is thickness noise and $p'_L(x,t)$ is loading noise.

Taking inflow into account, convective FW–H equation should be [18]

$$\left[\frac{1}{c_0^2}\frac{D^2}{Dt^2}-\nabla^2\right]p'(x,t)H(f)=\frac{D}{Dt}Q\delta(f)-\frac{\partial}{\partial x_i}L_i\delta(f) +\frac{\partial^2}{\partial x_i\partial x_j}\left[T_{ij}H(f)\right], \tag{8}$$

where

$$\frac{D}{Dt}=\frac{\partial}{\partial t}+U_{\infty i}\frac{\partial}{\partial x_i}, \tag{9}$$

$$Q=\rho_0(v_n-U_{\infty n})+\rho[u_n-(v_n-U_{\infty n})], \tag{10}$$

$$L_i=\left[(p-p_0)\delta_{ij}-\sigma_{ij}\right]n_j+\rho u_i[u_n-(v_n-U_{\infty n})], \tag{11}$$

$$T_{ij}=\rho u_i u_j+\left[(p-p_0)-c_0^2(\rho-\rho_0)\right]\delta_{ij}-\sigma_{ij}, \tag{12}$$

With equations (9)–(12), the analytical solutions of convective FW–H equation can be obtained as

$$\begin{aligned}4\pi p'_T(x,t)=&\int_S\left[\frac{(1-M_{\infty R})\dot{Q}}{R^*(1-M_R)^2}\right]_{\text{ret}}\mathrm{d}S-\int_S\left[\frac{c_0M_{\infty R^*}Q}{R^{*2}(1-M_R)}\right]_{\text{ret}}\mathrm{d}S\\ &+\int_S\left[(1-M_{\infty R})Q\frac{R^*\dot{M}_R+c_0\left(M_{R^*}-|\boldsymbol{M}|^2\right)}{R^{*2}(1-M_R)^3}\right]_{\text{ret}}\mathrm{d}S\\ &-\int_S\left[(1-M_{\infty R})Q\frac{c_0M_{R^*}M_R+c_0\gamma^2\left(M_{\infty M}^2-M_{R^*}^2\right)}{R^{*2}(1-M_R)^3}\right]_{\text{ret}}\mathrm{d}S\\ &-\int_S\left[\frac{c_0\gamma^2\left(M_{\infty R^*}M_{R^*}-M_{\infty M}^2\right)Q}{R^{*2}(1-M_R)^2}\right]_{\text{ret}}\mathrm{d}S\end{aligned} \tag{13}$$

$$\begin{aligned}4\pi p'_L(x,t)=&\frac{1}{c_0}\int_S\left[\frac{\dot{L}_R}{R^*(1-M_R)^2}\right]_{\text{ret}}\mathrm{d}S-\int_S\left[\frac{L_{R^*}-L_M}{R^{*2}(1-M_R)^2}\right]_{\text{ret}}\mathrm{d}S\\ &+\frac{1}{c_0}\int_S\left[L_R\frac{R^*\dot{M}_R+c_0\left(M_{R^*}-|\boldsymbol{M}|^2\right)}{R^{*2}(1-M_R)^3}\right]_{\text{ret}}\mathrm{d}S\end{aligned}$$

$$-\int_S \left[L_R \frac{M_{R^*} M_R + \gamma^2 \left(M_{\infty M}^2 - M_{R^*}^2\right)}{R^{*2}(1-M_R)^3} \right]_{\text{ret}} \mathrm{d}S$$

$$-\int_S \left[\frac{L_{R^*} M_R + \gamma^2 \left(M_{\infty M} M_{\infty L} - L_{R^*} M_{R^*}\right)}{R^{*2}(1-M_R)^2} \right]_{\text{ret}} \mathrm{d}S, \quad (14)$$

where

$$\begin{aligned} R^* &= \tfrac{1}{\gamma}\sqrt{r^2 + \gamma^2(\boldsymbol{M}_\infty \cdot \boldsymbol{r})} \\ R &= \gamma^2(R^* - \boldsymbol{M}_\infty \cdot \boldsymbol{r}) \\ \gamma &= \sqrt{\tfrac{1}{1-M_\infty^2}} \end{aligned} \quad (15)$$

and

$$\boldsymbol{r} = r_{\text{ob}} - r_{\text{i}}. \quad (16)$$

Equation (16) indicates the vector from the sound source point on the surface of the blade to the observe point.

When $M_\infty = 0$, convective FW–H equation is the same as FW–H equation. By comparing FW–H equation and convective FW–H equation, the difference caused by inflow Mach number M_∞ can be obtained as

$$4\pi p'_{T(M_\infty)}(x,t) = -\int_S \left[\frac{\dot{Q} M_{\infty R}}{R^*(1-M_R)^2} \right]_{\text{ret}} \mathrm{d}S - \int_S \left[\frac{c_0 Q M_{\infty R^*}}{R^{*2}(1-M_R)} \right]_{\text{ret}} \mathrm{d}S$$

$$-\int_S \left[Q M_{\infty R^*} \frac{R^* \dot{M}_R + c_0 \left(M_{R^*} - |\boldsymbol{M}|^2\right)}{R^{*2}(1-M_R)^3} \right]_{\text{ret}} \mathrm{d}S$$

$$-\int_S \left[(1-M_{\infty R}) Q \frac{c_0 M_{R^*} M_R + c_0 \gamma^2 \left(M_{\infty M}^2 - M_{R^*}^2\right)}{R^{*2}(1-M_R)^3} \right]_{\text{ret}} \mathrm{d}S$$

$$-\int_S \left[\frac{c_0 \gamma^2 \left(M_{\infty R^*} M_{R^*} - M_{\infty M}^2\right) Q}{R^{*2}(1-M_R)^2} \right]_{\text{ret}} \mathrm{d}S, \quad (17)$$

$$4\pi p'_{L(M_\infty)}(x,t) = -\int_S \left[L_{R^*} \frac{M_{R^*} M_R + \gamma^2 \left(M_{\infty M}^2 - M_{\text{R}^*}^2\right)}{R^{*2}(1-M_R)^3} \right]_{\text{ret}} \mathrm{d}S$$

$$-\int_S \left[\frac{L_{R^*} M_R + \gamma^2 \left(M_{\infty M} M_{\infty L} - L_{R^*} M_{R^*}\right)}{R^{*2}(1-M_R)^2} \right]_{\text{ret}} \mathrm{d}S. \quad (18)$$

Therefore, equations (19) and (20) can be regarded as the influence index of inflow Mach, a quantificational expression of the affections of inflow Mach on thickness noise and loading noise.

2.2 BEM method

The common form of Helmholtz differential equation is:

$$\nabla^2 p - k^2 p = 0, \quad (19)$$

where p is the acoustic pressure, ∇^2 is the Laplace operator, $k = \omega / c_0$.

The relationship of the pressure derivative and local normal velocity can be described as:

$$\frac{\partial p}{\partial n} = i\omega\rho v_n. \quad (20)$$

At infinity, p must satisfy Sommerfeld radiation condition:

$$\lim_{r\to\infty}\left[r\left(\frac{\partial p}{\partial r} - ikp\right)\right] = 0. \quad (21)$$

The Green Function at free acoustic field can be introduced as:

$$G(Q,P) = \frac{e^{-ikr}}{4\pi r}, \quad (22)$$

where P is the observe point and Q is one of the field points $r = |Q - P|$.

Therefore the common form of Helmholtz boundary integral equation can be obtained as:

$$C(P)p(P) = \int_S \left(G(Q,P)\frac{\partial p(Q)}{\partial n} - \frac{\partial G(Q,P)}{\partial n} p(Q)\right)\mathrm{d}S(Q), \quad (23)$$

where

$$C(P) = \begin{cases} 1 & P \in D' \\ 1 - \int_S \dfrac{\cos\beta}{4\pi r^2}\mathrm{d}S(Q) & P \in S \\ 0 & P \notin (\mathrm{S} \cup D') \end{cases}, \quad (24)$$

$$\frac{\partial p}{\partial n} = -\mathrm{i}\omega\rho v_n(Q), \quad (25)$$

$$\frac{\partial G(Q,P)}{\partial n} = \frac{e^{-\mathrm{i}kr}}{4\pi r}\left(\mathrm{i}k + \frac{1}{r}\right)\cos\beta. \quad (26)$$

The total acoustic pressure equals to the summation of incoming acoustic pressure and scatter acoustic pressure:

$$p = p_i + p_s. \quad (27)$$

For plain wave, incoming acoustic pressure appears as:

$$p_i = A e^{-\mathrm{i}k(\alpha x + \beta y + \gamma z)}. \quad (28)$$

For spherical wave, incoming acoustic pressure appears as:

$$p_i = B\frac{e^{-\mathrm{i}kR}}{R}. \quad (29)$$

When p_s is used in Helmholtz boundary integral equation, we can obtain that

$$C(P)p(P) = -\int_S \left(\mathrm{i}\rho\omega v_n^s G - p_s\frac{\partial G}{\partial n}\right)\mathrm{d}S. \quad (30)$$

When p_i is used in Helmholtz boundary integral equation, we can obtain that

$$C^0(P)p_i(P) = -\int_S \left(\mathrm{i}\rho\omega v_n^i G - p_i\frac{\partial G}{\partial n}\right)\mathrm{d}S. \quad (31)$$

Subtracting equation (31) from equation (30) and combining with equation (27), we can obtain

$$C(P)[p(P)-p_i(P)]-C^0(P)p_i(P) = -\int_S\left(\mathrm{i}\rho\omega v_n G - p\frac{\partial G}{\partial n}\right)\mathrm{d}S, \quad (32)$$

where

$$C(P)+C^0(P)=1. \quad (33)$$

Thus equation (32) can be simplified as

$$C(P)p(P) = -\int_S\left(\mathrm{i}\rho\omega v_n G - p\frac{\partial G}{\partial n}\right)\mathrm{d}S + p_i(P). \quad (34)$$

In equation (34), $p_i(P)$ is the incidence pressure calculated by convective FW–H equation. $C(P)$ can be obtained by equation (24). For the integral items. G is the Green function and $\boldsymbol{n}$ is the unit normal vector of a surface element.

2.3 Calculation of the sound pressure gradient

In equation (34), $\mathrm{i}\rho\omega v_n$ is the sound pressure gradient that is obtained from equation (25). The sound pressure gradient can be calculated by equation (35) [23]

$$\frac{p(x,\,t,\,\boldsymbol{M}_\infty)}{\partial x_i} = \frac{p_\alpha(x,\,t,\,\boldsymbol{M}_\infty)}{\partial x_i} + \frac{\partial p'_\beta(x,\,t,\,\boldsymbol{M}_\infty)}{\partial x_i}, \quad (35)$$

where

$$4\pi\frac{\partial p'_\alpha(x,\,t,\,\boldsymbol{M}_\infty)}{\partial x_i} = \frac{\partial}{\partial \mathrm{t}}\frac{\partial}{\partial x_i}\int_{-\infty}^{t}\int_{\mathrm{S}}\mathrm{Q}\frac{\delta(g)}{R^*}\mathrm{d}S\mathrm{d}T, \quad (36)$$

$$4\pi\frac{\partial p'_\alpha(x,\,t,\,\boldsymbol{M}_\infty)}{\partial x_i} = -\frac{\partial^2}{\partial x_i^2}\int_{-\infty}^{t}\int_{\mathrm{S}}F_i\frac{\delta(g)}{R^*}\mathrm{d}S\mathrm{d}T. \quad (37)$$

A further simplification can obtain the analytical expression of the sound pressure gradient of convective FW–H equation

$$4\pi\frac{\partial p'_\alpha(x,\,t,\,\boldsymbol{M}_\infty)}{\partial x_i} = I_1+I_2+I_3+I_4+I_5, \quad (38)$$

$$4\pi\frac{\partial p'_\beta(x,\,t,\,\boldsymbol{M}_\infty)}{\partial x_i} = I_6+I_7+I_8+I_9+I_{10}+I_{11}+I_{12}, \quad (39)$$

where

$$I_1 = -\frac{1}{c_0}\int_S\left[\ddot{Q}\tilde{R}_iU(1,3)+\dot{Q}\dot{\tilde{R}}_iU(1,3)+\dot{Q}\tilde{R}_iV(1,2)U(0,\,1)\right]_e\mathrm{d}S, \quad (40)$$

$$I_2 = -\frac{1}{c_0}\int_S\left[\dot{Q}\tilde{R}_iU(2,4)W+Q\dot{\tilde{R}}_iU(2,4)W+Q\tilde{R}_iV(2,3)U(0,\,1)W+Q\tilde{R}_iU(2,4)\dot{W}\right]_e\mathrm{d}S, \quad (41)$$

$$I_3 = -\frac{1}{c_0}\int_S\left[\dot{Q}\tilde{R}_iU(2,4)Z+Q\dot{\tilde{R}}_iU(2,4)Z+Q\tilde{R}_iV(2,3)U(0,\,1)Z+Q\tilde{R}_iU(2,4)\dot{Z}\right]_e\mathrm{d}S \quad (42),$$

$$I_4 = \int_S\left[\dot{Q}\tilde{R}_i^*U(2,2)+Q\dot{\tilde{R}}_i^*U(2,2)+Q\tilde{R}_i^*V(2,1)U(0,\,1)\right]_e\mathrm{d}S, \quad (43)$$

$$I_5 = -\int_S\left[\dot{Q}B_iU(2,3)+Q\dot{B}_iU(2,3)+QB_iV(2,2)U(0,\,1)\right]_e\mathrm{d}S, \quad (44)$$

$$I_6 = -\frac{1}{c_0^2}\int_S\left[\left(\frac{\partial\dot{F}_R}{\partial t}\right)\tilde{R}_iU(1,3)+\dot{F}_R\dot{\tilde{R}}_iU(1,3)+\dot{F}_R\tilde{R}_iV(1,2)U(0,\,1)\right]_e\mathrm{d}S, \quad (45)$$

$$I_7 = -\frac{1}{c_0}\int_S\left[\dot{A}_iU(2,3)+A_iV(2,2)U(0,\,1)\right]_e\mathrm{d}S, \quad (46)$$

$$I_8 = -\frac{1}{c_0}\int_S\left[\left(\frac{\partial F_R}{\partial t}\right)B_iU(2,3)+F_R\dot{B}_iU(2,3)+F_RB_iV(2,2)U(0,\,1)\right]_e\mathrm{d}S, \quad (47)$$

$$I_9 = -\frac{1}{c_0^2}\int_S\left[\left(\frac{\partial F_R}{\partial t}\right)\tilde{R}_iDU(2,4)+F_R\dot{\tilde{R}}_iDU(2,4)\right]_e\mathrm{d}S - \frac{1}{c_0^2}\int_S\left[F_R\tilde{R}_i\dot{D}U(2,4)+F_R\tilde{R}_iDV(2,3)U(0,1)\right]_e\mathrm{d}S, \quad (48)$$

$$I_{10} = \frac{1}{c_0}\int_S\left[\left(\frac{\partial F_R}{\partial t}\right)\tilde{R}_iHU(2,4)+F_R\dot{\tilde{R}}_iHU(2,4)\right]_e\mathrm{d}S + \frac{1}{c_0}\int_S\left[F_R\tilde{R}_i\dot{H}U(2,4)+F_R\tilde{R}_iHV(2,3)U(0,1)\right]_e\mathrm{d}S, \quad (49)$$

$$I_{11} = \frac{1}{c_0}\int_S\left[\dot{K}_iU(2,2)+K_iV(2,1)U(0,1)\right]_e\mathrm{d}S, \quad (50)$$

$$I_{12} = \int_S\left[\left(\frac{1}{\gamma^2}\right)F_i+M_{\infty i}M_{\infty F}-3\tilde{R}_i^*F_{R^*}\right]\mathrm{U}(3,\,1)\mathrm{d}S. \quad (51)$$

The elements mentioned above are all known qualities and the only unknown quality is the total sound pressure p, which is the solution target.

2.4 Matrix form of the sound pressure calculation

The discretization of the integral can transfer equations (34)–(52):

$$\sum_{j=1}^{N}\left(C(P)p_j(P)\right) = -\sum_{j=1}^{N}\left(\mathrm{i}\rho\omega v_n^j G\mathrm{d}S_j - p_j(P)\frac{\partial G}{\partial n_j}\mathrm{d}S_j\right) + \sum_{j=1}^{N} p_i^j(P). \tag{52}$$

Based on the same surface element $\mathrm{d}S_j$, every integral/summation element marked j on the left of the equal sign in equation (52) equals to the one marked j on the right side. Therefore equation(52) can be written as:

$$\left(C(P)+\frac{\partial G}{\partial n_j}\mathrm{d}S_j\right)p_j(P) = p_i^j(P) - \mathrm{i}\rho\omega v_n^j G\mathrm{d}S_j, \quad j = 1,2,3,...,N. \tag{53}$$

Equation (36) can be written as the matrix form:

$$\begin{bmatrix} \alpha_1 & & 0 \\ & \alpha_2 & \\ & \ddots & \\ 0 & & \alpha_N \end{bmatrix}\begin{bmatrix} p_1 \\ p_2 \\ \vdots \\ p_N \end{bmatrix} = \begin{bmatrix} \beta_1 \\ \beta_2 \\ \vdots \\ \beta_N \end{bmatrix}, \tag{54}$$

where

$$\begin{cases} \alpha_j = C(P) + \dfrac{\partial G}{\partial n_j}\mathrm{d}S_j, \\ \beta_j = p_i^j(P) - \mathrm{i}\rho\omega v_n^j G\mathrm{d}S_j. \end{cases} \tag{55}$$

Let $\boldsymbol{A} = \begin{bmatrix} \alpha_1 & & 0 \\ & \alpha_2 & \\ & \ddots & \\ 0 & & \alpha_N \end{bmatrix}$, $\boldsymbol{p} = [\,p_1 \quad p_2 \quad \cdots \quad p_N\,]^{\boldsymbol{T}}$, $\boldsymbol{b} = [\,\beta_1 \quad \beta_2 \quad \cdots \quad \beta_N\,]^{\boldsymbol{T}}$.

Equation (37) can be written as the form of:

$$\begin{cases} \boldsymbol{Ap} = \boldsymbol{b}, \\ \boldsymbol{p} = \boldsymbol{A}^{-1}\boldsymbol{b}. \end{cases} \tag{56}$$

Then the total sound pressure vector $\boldsymbol{p}$ can be obtained by equation (56), which is known as the matrix form of the sound pressure calculation.

3. Models and simulation environments

3.1 Geometry models of the helicopters

The geometry models of the fuselages are established by adopting the parametric modeling method (PMM), combined with the real fuselage shape. Main geometry parameters of the fuselages are confirmed as the decisive factors of the helicopter fuselage and the rotor.

Figure 1 shows the three-view drawing of the simplified helicopter geometry model and the main decisive parameters are outlined. L_h is the length of the whole helicopter. L_f is the length of the main body of fuselage. W_f is the width of the fuselage. H_f is the height of the fuselage. H_r is the height of the rotor that refers to the distance from the coordinate origin to the center of rotor. R_r is the radius of the rotor. L_b is the length of the blades.

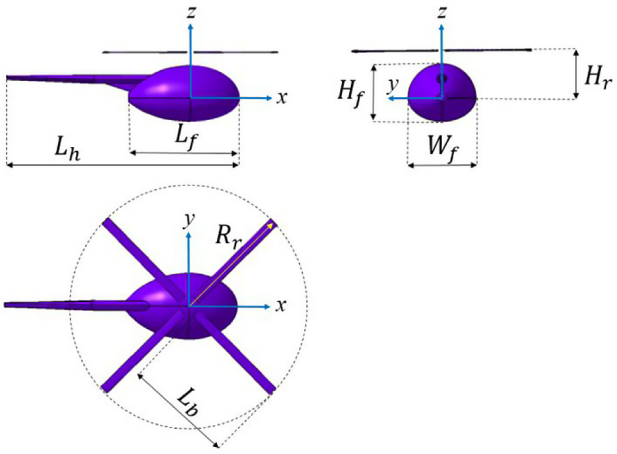

Figure 1. Establishment of the simplified helicopter geometry model (including rotor and fuselage).

Table 1. Nomenclature of the physical quantities.

Symbols	Physical quantities
L_h	Length of the whole helicopter
L_f	Length of the main body of fuselage
W_f	Width of the fuselage
H_f	Height of the fuselage
H_r	Height of the rotor
R_r	Radius of the rotor
L_b	Length of the blades

The parameters listed in Figure 1 and Table 1 can be the main geometry parameters of the approximate design of a helicopter. The size and shape of the helicopter can be preliminary determined with the main geometry parameters and the primary geometry model of the helicopter can be given. Then the primary geometry model can be corrected to the final geometry model according to other detailed information.

Three typical helicopter fuselage, OH-6, HUEY and RAH-66, are selected for the research on the scattering effect of different fuselage types.

The OH-6 fuselage model established in this paper is shown in Figure 2, according to the design of the OH-6 helicopter [24]. The model mainly includes the main part of the OH-6 fuselage while the tail of the fuselage is simplified.

The HUEY fuselage model established in this paper is shown in Figure 3, according to the design of the HUEY helicopter [25]. The fuselage model mainly includes the main part of the OH-6 fuselage while the tail of the fuselage is simplified.

The RAH-66 fuselage model established in this paper is shown in Figure 4, according to the design of the RAH-66 stealth helicopter [26]. The fuselage model mainly includes the main part of the OH-6 fuselage while the tail of the fuselage is simplified.

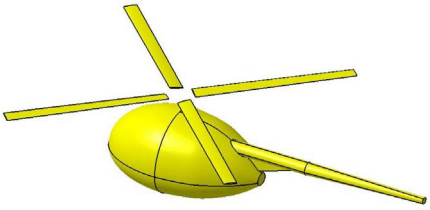

Figure 2. Helicopter model with OH-6 fuselage.

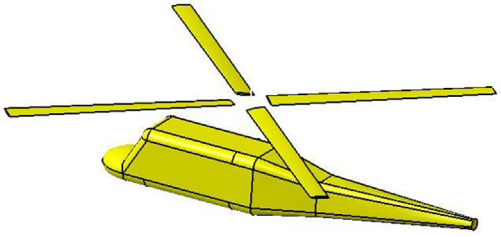

Figure 3. Helicopter model with HUEY fuselage.

In the simulation case shown in Figure 5, the acoustic noise detector receives the acoustic noise waves produced by helicopter at the pitching angle $\theta = 45°$, and the azimuth angle from 0° to 360°. The distance from the helicopter to the detector is 10 m. The inflow Mach number is $M_\infty = 0.2$.

4. Results and discussions

4.1 Approach to the results

In this paper, the theories and the methodologies enumerated in Section 2 are used for the calculation of the acoustic noise generated by the helicopter rotor and the scattering effects of the helicopter fuselage. Figure 6 is created to intuitively illustrate the whole progress from the model establishment to the result calculation, and also the combination of the methodologies and the results.

According to Figure 6, the methodology approach to the final results (sound pressure and SPL) can be described as 4 steps.

Step 1: Establishment of simulation environment.

Environment parameters, as is shown in Figure 4, is fixed in this step. The environment parameters mainly includes the relative location and the distance from the helicopter to the observer, the height and attitude angles of the helicopter, and the flight speed (inflow Mach number, M_∞) of the helicopter, reflecting the whole simulation environment.

Step 2: Establishment of geometry model and mesh generation.

Main geometry parameters mentioned in Section 3 is assigned in this step for the design of the helicopter geometry models. The size and the primary shape can be figured out by the main geometry parameters, and then the shape

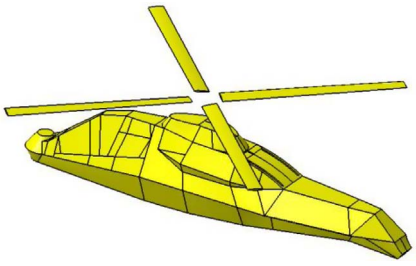

Figure 4. Helicopter model with RAH-66 fuselage.

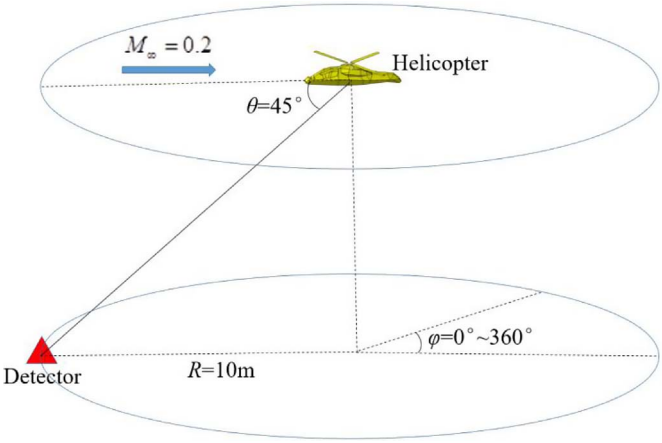

Figure 5. Schematic of simulation case.

is finally decided by the detailed information such as the airfoil of the blades, the specific shape of the fuselage, etc. Mesh generation is operated after the establishment of the geometry models, for the discretization of the surfaces of the models.

Step 3: Application of method based on FW–H and BEM.

The combined methodology mainly consisting of FW–H equation and BEM helps transfer the geometry models under the specific environment into the matrixes for calculations. Firstly, the acoustic noise generated by the rotor and the sound pressure gradient is obtained by using convective FW–H equation. Then BEM is applied for the acquisition of the Green Function, the surface normal vector, etc. Finally, the acquired physical quantities are recombined into the matrixes for calculations.

Step 4: Calculation of sound pressure and SPL.

After the acquisition of the matrixes for calculations, the calculations of the final results can be easily carried out by program languages. The sound pressure of the rotor noise can be firstly obtained and the sound pressure levels (SPL) can be obtained by Fourier transformation.

4.2 Influence of fuselage types

The scattering effects of different fuselage types can be observed from Figures 7 and 8.

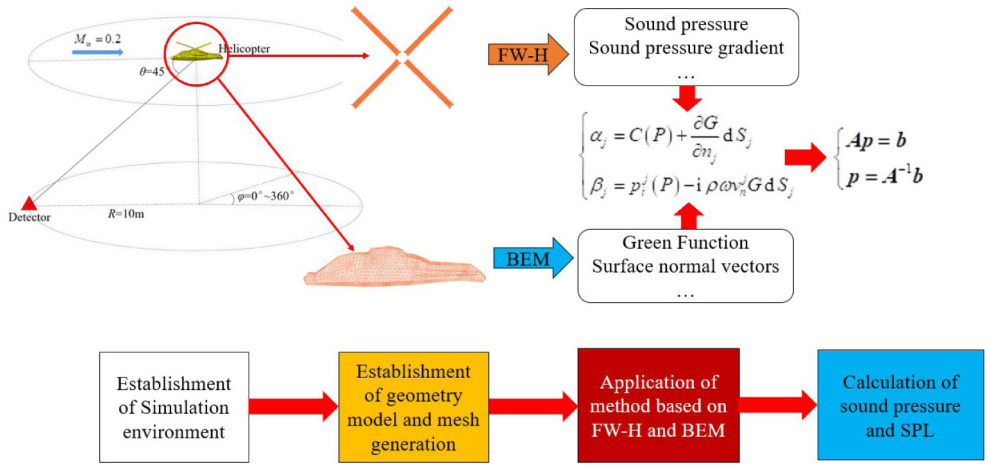

Figure 6. Schematic diagram and flow chat of the methodology approach.

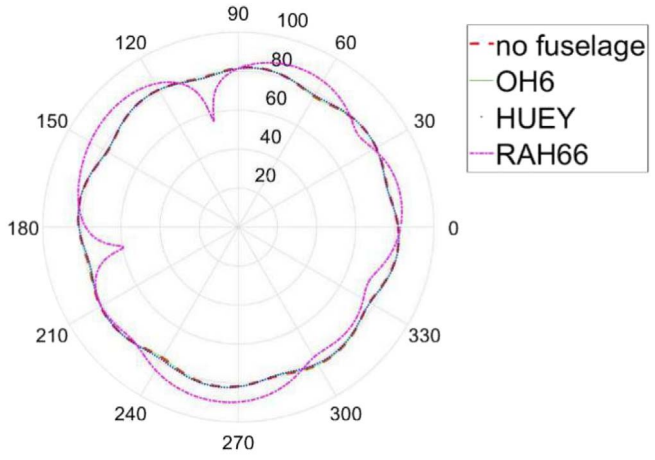

Figure 7. Scattering effects of different types of fuselage (polar graph).

It can be illustrated from Figures 7, 8 and Table 2 that fuselage RAH-66 has more obvious scattering effects than the other two traditional fuselages, OH-6 and HUEY, with the superiority of 2.79 dB in total sound pressure level and 7.47 dB in maximum sound pressure level, indicating that the acoustic noise scattering effects vary from different fuselage types.

As a type of radar-stealth fuselage, RAH-66 fuselage consists of pieces of plains, causing sharp edges on the fuselage surface. OH-6 fuselage and HUEY fuselage, however, are made up of smooth surfaces with few sharp edges. Thus an inference can be presented that the sharp edges of a helicopter fuselage can cause obvious acoustic scattering effects.

For the verification of the inference above, another two helicopter models are established, one equipped with cuboid fuselage with sharp edges and the other equipped with capsule fuselage without sharp edges, as is shown in Figures 9 and 10.

The acoustic scattering effects of cuboid and capsule fuselage are shown in Figures 11 and 12.

It can be obtained from Figures 11, 12 and Table 3 that the sound pressure level of acoustic noise scattered by cuboid fuselage apparently differs from that of the rotor blades while the acoustic noise scattered by capsule fuselage is almost the same as that of the rotor blades, verifying that helicopter fuselages with substantial sharp edges causes more obvious scattering effects.

4.3 Influence of radius of curvature of fuselage sharp edges

For quantitative studies on the influences of fuselage sharp edges, the radius of curvature (RC) of fuselage sharp edges is introduced. The variation progress from the cuboid fuselage to the capsule fuselage can be regarded to be the increase of RC of fuselage sharp edges, as is shown in Figure 13.

For the cuboid fuselage mentioned above, the RC of the sharp edges is fixed at 100 mm, 200 mm, 300 mm, 400 mm and 500 mm, and the scattering effects of these fuselages with different RC is calculated by the method based on FW–H equation and BEM.

The acoustic scattering effects of cuboid fuselages with different RC are shown in Figure 14.

From Table 4, it can be seen that with the increase of RC, the maximum SPL shows monotone decreasing while the total SPL changes irregularly. It can be indicated from the variation of the maximum SPL that the increase of RC of the fuselage sharp edges makes contributions to the suppression of the fuselage scattering effects. As for the total SPL, it can reflects the approximate level of the SPL. However, its variation tendencies cannot reflect the influence on the scattering effects. The reason can be described that the existence of the outlier points such as some obviously low minimum points can pull down the average value, causing that the data group with higher maximum SPL and more significant scattering effects might have lower total SPL.

In order to preliminarily find the function relationship between the RC of the fuselage sharp edge and the maximum SPL, several assumptions are made according

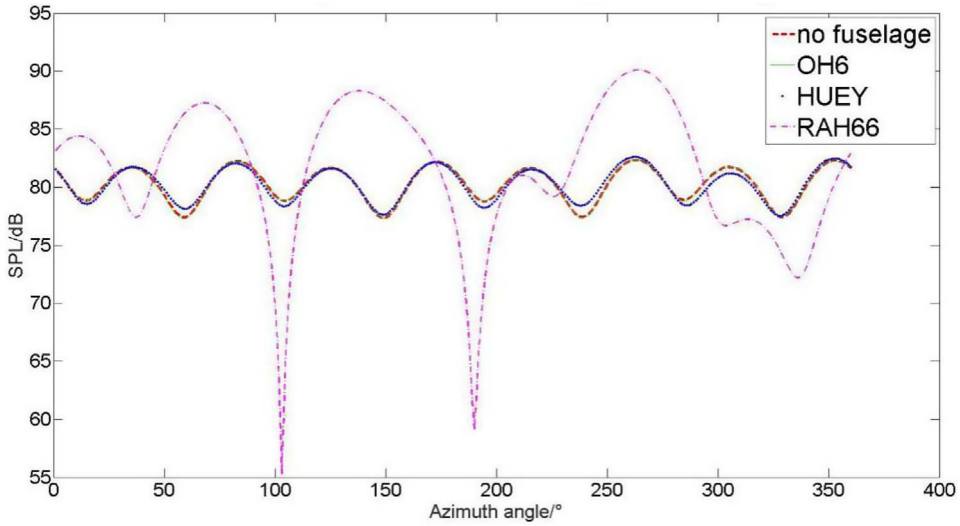

Figure 8. Scattering effects of different types of fuselage (XY graph).

Table 2. Total and maximum SPL of helicopters with different fuselages.

Fuselage	No fuselage	OH-6	HUEY	RAH-66
Total sound pressure level/dB	80.35	80.35	80.35	83.14
Maximum sound pressure level/dB	82.33	82.35	82.62	90.09

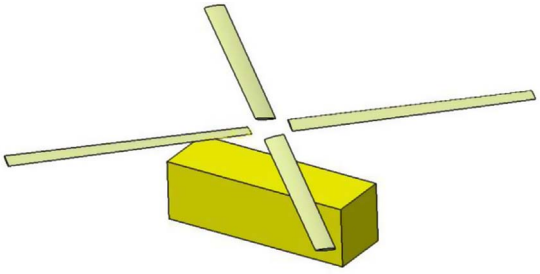

Figure 9. Helicopter model with cuboid fuselage.

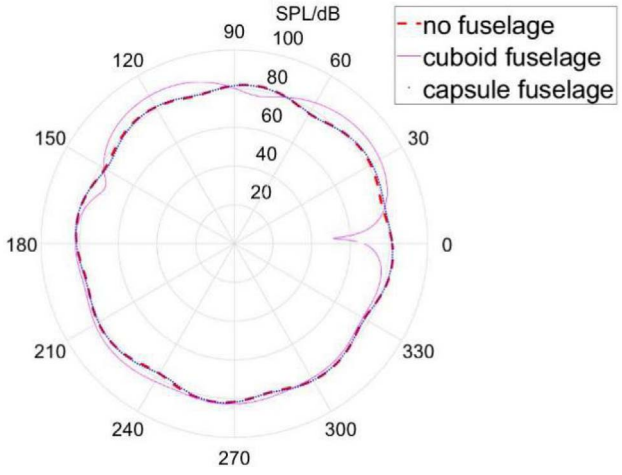

Figure 10. Helicopter model with capsule fuselage.

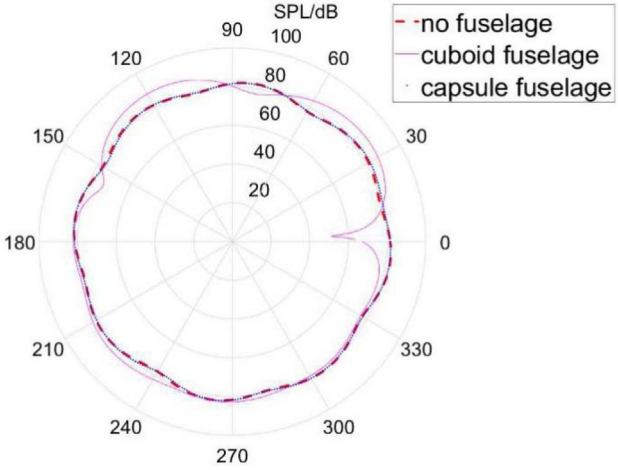

Figure 11. Acoustic noise scattering effects of cuboid fuselage and capsule fuselage.

to the shapes of SPL–RC graph, (1/SPL) –RC graph, etc. It is finally discovered that $Y = Y(\mathrm{SPL})$ is linear with $X = X(\mathrm{RC})$, which can be described as:

$$\begin{cases} Y = \frac{1}{\mathrm{SPL}} \\ X = \ln(\mathrm{RC} + a)\,. \\ Y = kX + b \end{cases} \tag{57}$$

In equation (57), SPL represents the maximum sound pressure level and RC represents the radius of curvature. Coefficients waiting for determination are a, b and k.

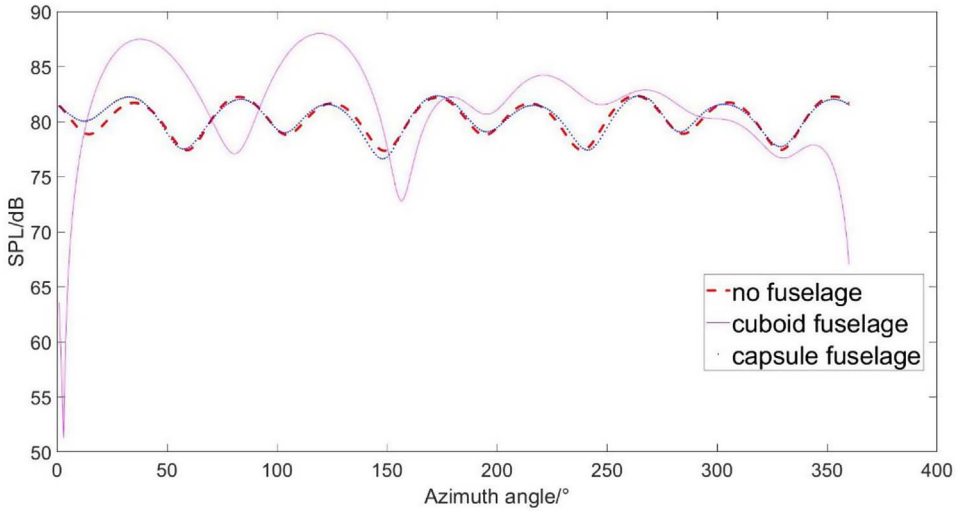

Figure 12. Acoustic noise scattering effects of cuboid fuselage and capsule fuselage.

Table 3. Total and maximum SPL of helicopters with cuboid and capsule fuselages.

Fuselage	No fuselage	Cuboid	Capsule
Total sound pressure level/dB	80.35	82.28	80.40
Maximum sound pressure level/dB	82.33	87.99	82.33

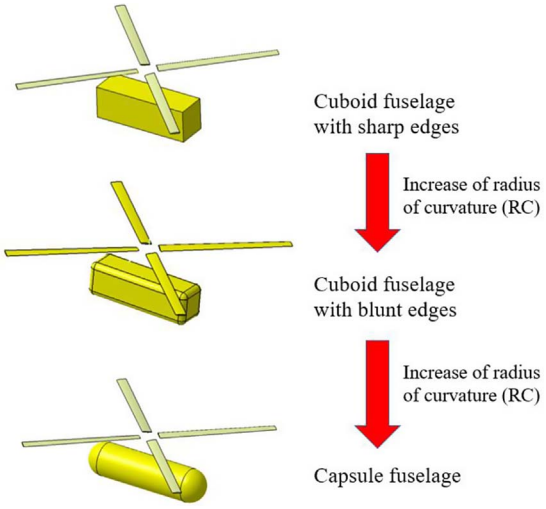

Figure 13. Effects of the increase of RC of fuselage sharp edges.

Figure 15 shows the scatter diagram of Y and X, indicating the linear relationship between them. According to least square method, the linear fitting equation can be obtained as

$$Y = 3.245 \times 10^{-4} X + 0.01016 \tag{58}$$

with

$$\begin{cases} a = 40 \\ b = 0.01016 \\ k = 3.245 \times 10^{-4} \end{cases}. \tag{59}$$

Besides, we can obtain the linearity relevance modulus equals to 0.9936, verifying the linear relationship between Y and X.

Therefore the estimated function relationship can be described as

$$\mathrm{SPL} = \frac{1}{3.245 \times 10^{-4}(\ln \mathrm{RC} + 40) + 0.01016}, \tag{60}$$

where the unit of *SPL* is dB and the unit of RC is mm.

The estimated function relationship shows the approximate variation law of the maximum SPL related to the radius of curvature of fuselage sharp edges, and can be used for the estimation for the scattering effects of fuselages with similar shapes but different radius of curvature of fuselage sharp edges.

4.4 Influence of length, width and height of the fuselage

As is shown in Figures 16–18, 12 other models are established based on RAH-66 model for the research on the variation effects of helicopter fuselage's length, width and height. In Figure 16, the length of the fuselage is multiplied by 0.8, 0.9, 1.1, 1.2. In Figure 17, the width of the fuselage is multiplied by 0.8, 0.9, 1.1, 1.2. In Figure 18, the height of the fuselage is multiplied by 0.8, 0.9, 1.1, 1.2.

The scattering effect of fuselages of different length ratios is shown in Figure 19 and Table 4.

Figure 19 indicates that the scattering effects of fuselages with different length obviously differ from each other. Besides, the scattering effects appear to be more significant with a longer fuselage. It can also be seen from Table 5 that

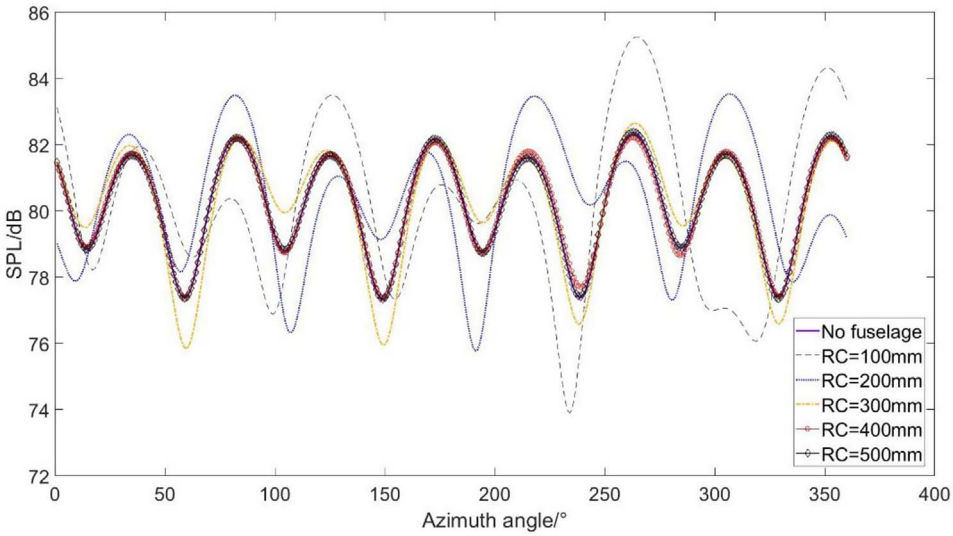

Figure 14. Acoustic scattering effects of cuboid fuselages with different RC.

Table 4. Maximum and total SPLs of helicopters with cuboid fuselages of different RC.

Radius of curvature (RC)/mm	Maximum SPL/dB	Total SPL/dB
0	87.99	82.28
100	85.26	83.36
200	83.53	79.19
300	82.65	81.61
400	82.38	81.65
500	82.22	81.58

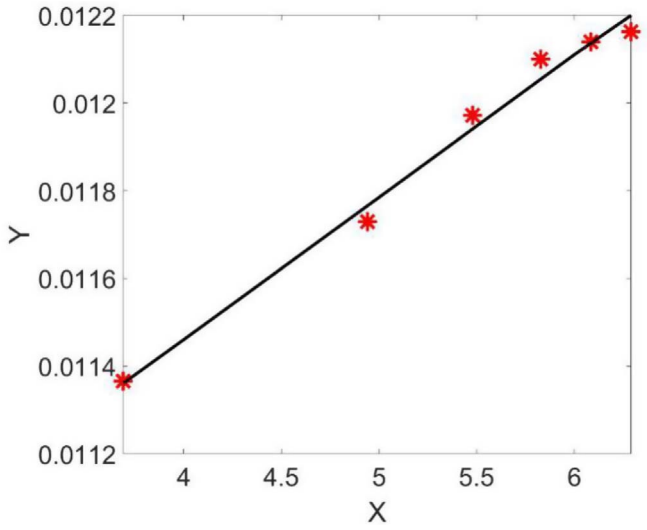

Figure 15. The scatter diagram and the linear fitting of Y and X.

the total sound pressure level and the maximum sound pressure level raises as the length of the fuselage increases. The main reason for the result can be illustrated that a longer fuselage has a larger scattering surface, letting more

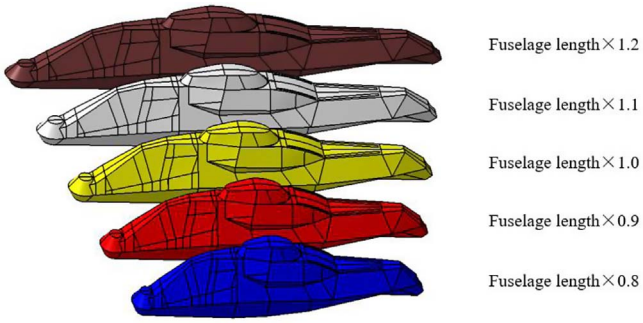

Figure 16. Fuselages with different length ratios.

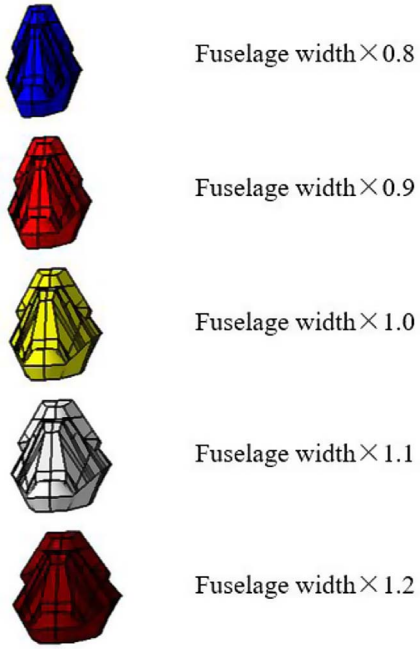

Figure 17. Fuselages with different width ratios.

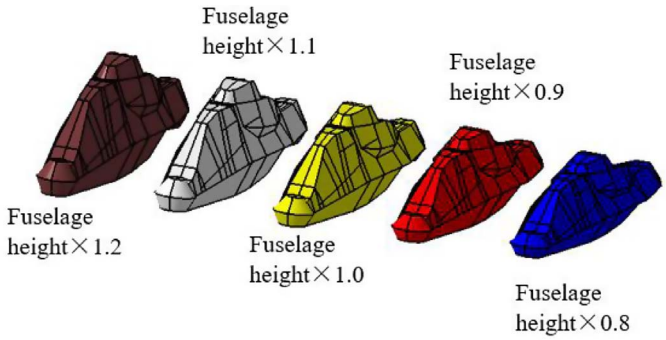

Figure 18. Fuselages with different height ratios.

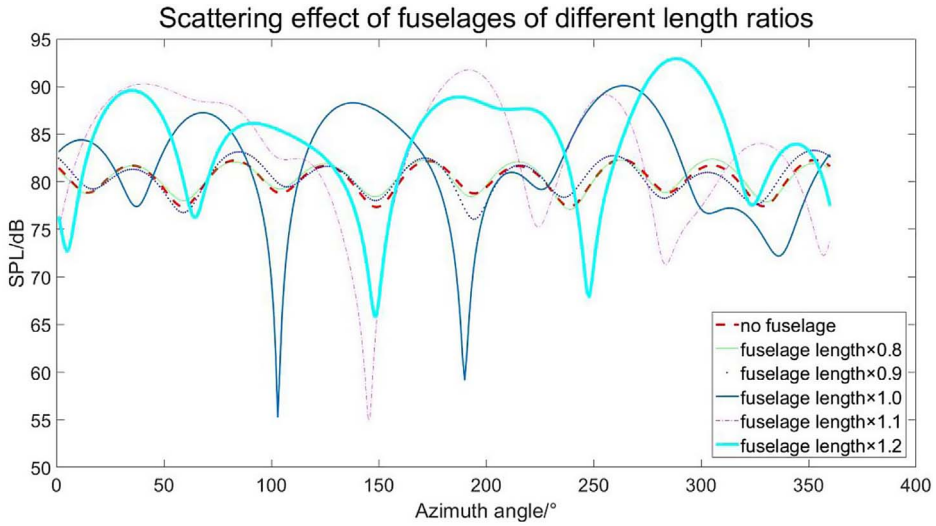

Figure 19. Scattering effect of fuselages of different length ratios.

Table 5. Total and maximum SPL of helicopters with fuselages of different length ratios.

Fuselage	No fuselage	Fuselage length × 0.8	Fuselage length × 0.9	Fuselage length × 1.0	Fuselage length × 1.1	Fuselage length × 1.2
Total sound pressure level/dB	80.35	80.51	80.51	83.14	84.79	85.34
Maximum sound pressure level/dB	82.33	82.38	83.29	90.09	91.74	92.91

sound waves reflect at the fuselage surface rather than propagate directly, and therefore make more chances for sound waves to get to the position of the detector.

The scattering effect of fuselages of different width ratios is shown in Figure 20 and Table 5.

The considerable difference of acoustic noise scattering effects can be seen from Figure 20 that the scattering effects of fuselages with different width. But the scattering effects seem not to be more significant with a wider fuselage. It can also be seen from Table 6 that the total sound pressure level and the maximum sound pressure level sometimes rise as the fuselage expands in width, but sometimes fall.

The scattering effect of fuselages of different height ratios is shown in Figure 21 and Table 7.

Similarly, the considerable difference of acoustic noise scattering effects can be seen from Figure 21 that the scattering effects of fuselages with different height. But the scattering effects seem not to be more significant with a higher fuselage. It can also be seen from Table 6 that the total sound pressure level and the maximum sound pressure level sometimes rise as the fuselage expands in height, but sometimes fall.

The main reason for this can be explained that the affection on the scattering effects of the normal directions

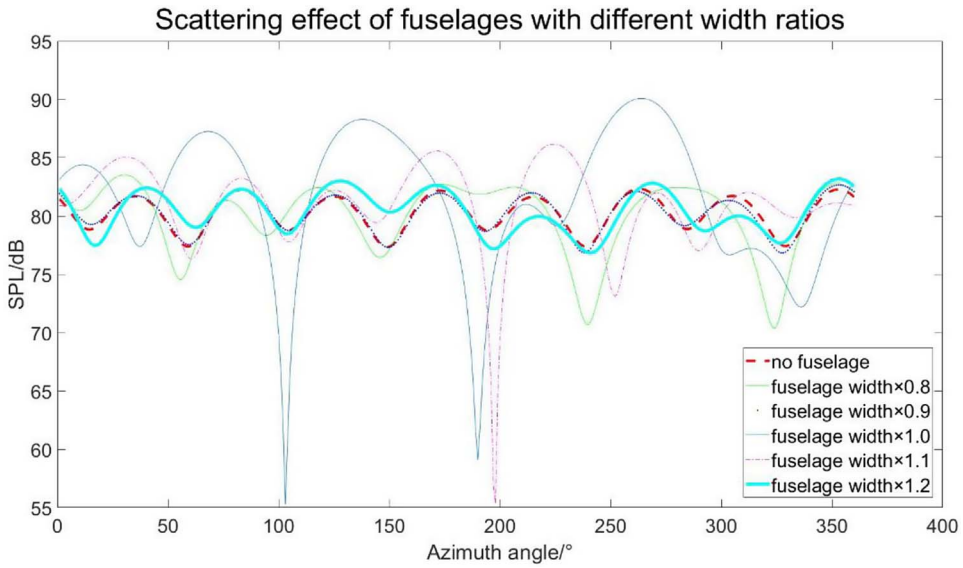

Figure 20. Scattering effect of fuselages with different width ratios.

Table 6. Total and maximum SPL of helicopters with fuselages of different width ratios.

Fuselage	No fuselage	Fuselage width × 0.8	Fuselage width × 0.9	Fuselage width × 1.0	Fuselage width × 1.1	Fuselage width × 1.2
Total sound pressure level/dB	80.35	80.38	80.37	83.14	81.53	80.54
Maximum sound pressure level/dB	82.33	83.53	82.66	90.09	86.16	83.17

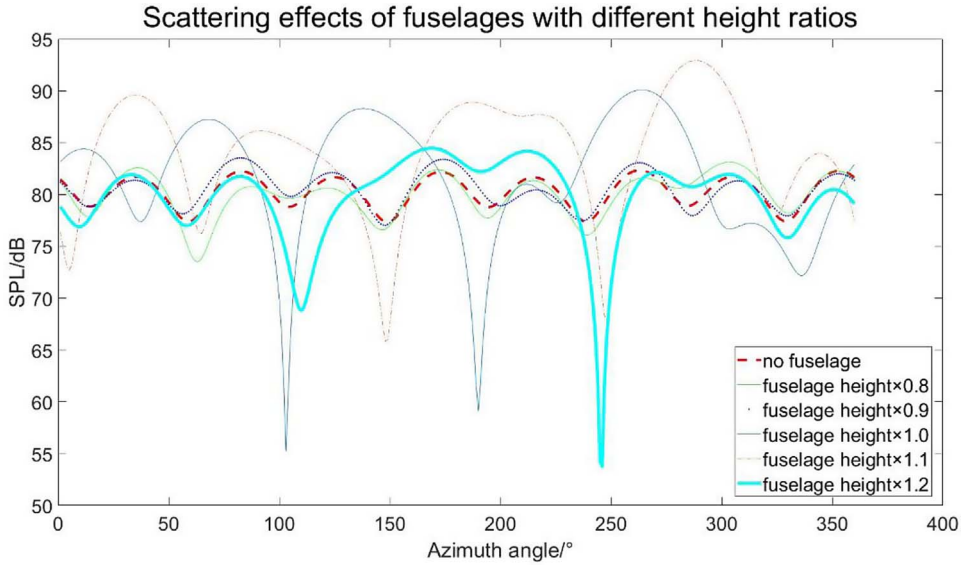

Figure 21. Scattering effect of fuselages with different height ratios.

of surface elements, which affect the travel directions of scattered sound waves, must be taken into consideration. Multiplied by the same ratio numbers, the change of width and height bring much more variations to surface element normal directions than the change of length. Thus the affection of the surface element normal directions cannot be ignored.

To sum up, the acoustic scattering effects of helicopter fuselage can be an essential element of acoustic stealth that cannot be ignored. Considering the acoustic stealth ability

Table 7. Total and maximum SPL of helicopters with fuselages of different height ratios.

Fuselage	No fuselage	Fuselage height × 0.8	Fuselage height × 0.9	Fuselage height × 1.0	Fuselage height × 1.1	Fuselage height × 1.2
Total sound pressure level/dB	80.35	80.17	80.61	83.14	85.35	85.35
Maximum sound pressure level/dB	82.33	83.12	83.52	90.09	92.91	84.46

of the designed helicopter, fuselages with massive sharp edges should be avoided. In addition, the length of helicopter fuselage should be limited and proper width and height of helicopter fuselage should be selected in order to take account of both acoustic stealth ability and capacity of helicopter fuselage.

Conclusions

Based on the presented FWH-BEM Method (FBM), the SPL of the noise generated by the rotor and scattered by the fuselage is predicted and the factors affecting the scattering effects are studied and discussed in detail. According to the results listed above, the following conclusions can be obtained:

1. The acoustic scattering effect of helicopter fuselage sometimes cannot be ignored for the reason that it varies with different types of fuselages, especially some radar-stealth fuselages. The total SPL of the acoustic noise of RAH-66 fuselage reaches 83.14 dB, with the superiority of 2.79 dB to that of OH-6 fuselage and HUEY fuselage.
2. Helicopter fuselages with sharp edges bring obvious scattering effects to the acoustic noise of helicopters while fuselages with few sharp edges have little scattering influence on the acoustic noise. The maximum SPL decreases when the RC of fuselage sharp edges increases. It can be obtained from the studies in this paper that for cuboid helicopter fuselages, the reciprocal of the maximum SPL is linear to the natural log of RC + a (a is a constant number). The estimated function relationship can be used for the estimation for the scattering effects of fuselages with similar shapes but different radius of curvature of fuselage sharp edges.
3. The length, width and height of helicopter fuselage can also be factors that affect the acoustic noise scattering effects. The scattering effect of a helicopter's acoustic noise appears to be more significant with a longer, wider or higher fuselage. Therefore the size of the helicopter should be limited, taking both the acoustic scattering and the volume of the fuselage into account.

Conflict of interest

The authors declare that they have no conflict of interest.

Acknowledgments

This work was supported by the National Natural Science Foundation of China (Grant No. 12004027).

References

1. D.Y. Dube, H.G. Patel: Suppressing the noise in measured signals for the control of helicopters. Fluctuation and Noise Letters 18, 1 (2019).
2. F. Liu, J. Lin, Y.Z. Wang: Design of cable parallel air-core coil sensor to reduce motion-induced noise in helicopter transient electromagnetic system. IEEE Transactions on Instrumentation and Measurement 68, 2 (2019) 525–532.
3. S. Hartjes, H.G. Visser: Optimal control approach to helicopter noise abatement trajectories in nonstandard atmospheric conditions. Journal of Aircraft 56, 1 (2019) 43–52.
4. S. Vouror, I. Goulos, C. Scullion: Impact of tip-vortex modeling uncertainty on helicopter rotor blade-vortex interaction noise prediction. Journal of the American Helicopter Society 66, 1 (2021) 1053–1065.
5. S. Vouros, I. Goulos, V. Pachidis: Integrated methodology for the prediction of helicopter rotor noise at mission level. Aerospace Science and Technology 89 (2019) 136–149.
6. L.Q. Wang, G.H. Xu, Y.J. Shi: Development and validation of a hybrid method for predicting helicopter rotor impulsive noise. Proceedings of the Institution of Mechanical Engineers Part G-Journal of Aerospace Engineering 233 (2019) 1323–1339.
7. J.E. Ffowcs Williams, D.L. Hawkings: Sound generation by turbulence and surface in arbitrary motion. Philosophical Transactions of the Royal Society A264, 1151 (1969) 321–342.
8. G. Ghorbaniasl, C. Lacor: A moving medium formulation for prediction of propeller noise at incidence. Journal of Sound and Vibration 331 (2012) 117–137.
9. G. Ghorbaniasl, L. Siozos-Rousoulis, C. Lacor: A time-domain Kirchhoff formula for the convective acoustic wave equation. Proceedings of the Royal Society A-Mathematical Physical and Engineering Sciences 472, 2187 (2016) 20150689.
10. Z.J. Huang, L. Siozos-Rousoulis, T.D. Troyer, G. Ghorbaniasl: A time-domain method for prediction of noise radiated from supersonic rotating sources in a moving medium. Proceedings of the Royal Society A-Mathematical Physical and Engineering Sciences 474, 2210 (2018) 20170089.
11. M.J. Bluck, S.P. Walker: Analysis of three-dimensional transient acoustic wave propagation using the boundary integral equation method. International Journal for Numerical Methods in Engineering 39 (1996) 1419–1431.
12. A.A. Ergin, B. Shanker, E. Michielssen: Analysis of transient wave scattering from rigid bodies using a Burton-Miller approach. Journal of the Acoustical Society of America 106, 5 (1996) 2396–2404.

13. D.J. Chappell, P.J. Harris, D. Henwood, R. Chakrabarti: A stable boundary element method for modeling transient acoustic radiation. Journal of the Acoustical Society of America 120, 1 (2006) 74–80.
14. R. Michel, K. Korcan: Near-and-far field modeling of advanced tail-rotor noise using source-mode expansions. Journal of Sound and Vibration 453 (2019) 328–354.
15. S. Lee, K. Brentner, P. Morris: Acoustic scattering in the time domain using an equivalent source method. AIAA Journal 48, 12 (2010) 2772–2780.
16. S. Lee, K.S. Brentner, P.J. Morris: Time-domain approach for acoustic scattering of rotorcraft noise. Journal of the American Helicopter Society 57, 4 (2012) 1–12.
17. N. Curle: The influence of solid boundaries upon aerodynamic sound. Proceedings of the Royal Society of London. Series A. Mathematical and Physical Sciences 231, 1187 (1955) 505–514.
18. O. Amoiridis, L. Siozos-Rousoulis, Z. Huang, N. Ricks, A. Kalfas, G. Ghorbaniasl: Aeroacoustic scattering of rotating sources using a frequency-domain acoustic pressure gradient formulation. Applied Acoustics 130 (2018) 99–106.
19. L. Siozos-Rousoulis, O. Amoiridis, Z. Huang, T. De Troyer, A.I. Kalfas, G. Ghorbaniasl: A convected frequency-domain equivalent source approach for aeroacoustic scattering prediction of sources in a moving medium. Journal of Sound and Vibration 431 (2018) 88–104.
20. S.A. Glegg: Airfoil self-noise generated in a cascade. AIAA Journal 36, 9 (1998) 1125–1182.
21. D. Casalino, M. Genito, A. Visingardi: Numerical analysis of airframe noise scattering effects in tilt rotor systems. AIAA Journal 45, 4 (2007) 751–759.
22. R.R. Mankbadi: Review of computational aeroacoustics in propulsion systems. Journal of Propulsion and Power 15, 4 (1999) 504–512.
23. Z.H. Wang, C.X. Bi, X.Z. Zhang, Y.B. Zhang: Sound field prediction and separation in a moving medium using the time domain equivalent source method. Acta Acustica United with Acustica 103, 3 (2017) 401–410.
24. D.Z. Suarez: Helicopters. Model World 3 (2020) 6–15.
25. A. Sehgal, E. Boyle: Design and development of a four-bladed tail rotor system for the USMC H-1 upgrade program. Journal of the American Helicopter Society 49, 2 (2004) 99–108.
26. A. Dobyns, B. Barr, J. Adelmann: RAH-66 Comanche building block structural qualification program. American Society for Testing and Materials Special Technical Publication 1383 (2001) 140–157.

Cite this article as: Wang Z. Huang J. & Yi M. 2022. Acoustic scattering effect prediction of helicopter fuselage based on BEM and convective FW–H equation. Acta Acustica, **6**, 24.